Where post-Newtonian and numerical-relativity waveforms meet

Mark Hannam,[1] Sascha Husa,[1] José A. González,[1,2] Ulrich Sperhake,[1] and Bernd Brügmann[1]

[1]*Theoretical Physics Institute, University of Jena, 07743 Jena, Germany*

[2]*Instituto de Física y Matemáticas, Universidad Michoacana de San Nicolás de Hidalgo, Edificio C-3, Cd. Universitaria. C. P. 58040 Morelia, Michoacán, Mexico*

(Received 2 July 2007; revised manuscript received 16 October 2007; published 13 February 2008)

We analyze numerical-relativity (NR) waveforms that cover nine orbits (18 gravitational-wave cycles) before merger of an equal-mass system with low eccentricity, with numerical uncertainties of 0.25 radians in the phase and 2% in the amplitude; such accuracy allows a direct comparison with post-Newtonian (PN) waveforms. We focus on waveforms predicted by one of the PN approximants that has been proposed for use in gravitational-wave data analysis, restricted 3.5PN TaylorT1, and compare these with a section of the numerical waveform from the second to the eighth orbit, which is about one and a half orbits before merger. This corresponds to a gravitational-wave frequency range of $M\omega = 0.0455$ to 0.1 Depending on the method of matching PN and NR waveforms, the accumulated phase disagreement over this frequency range can be within numerical uncertainty. Similar results are found in comparisons with an alternative PN approximant, 3PN TaylorT3. The amplitude disagreement, on the other hand, is around 6%, but roughly constant for all 13 cycles that are compared, suggesting that for the purpose of producing "hybrid waveforms," only 4.5 orbits need be simulated to match PN and NR waves with the same accuracy as is possible with nine orbits. If, however, we model the amplitude up to 2.5PN order, numerical and post-Newtonian amplitude disagreement is close to the numerical error of 2%.

DOI: 10.1103/PhysRevD.77.044020 PACS numbers: 04.25.D−, 04.30.Db, 95.30.Sf, 98.80.Jk

I. INTRODUCTION

The current generation of interferometric gravitational-wave (GW) detectors [1–3] have reached design sensitivity, and have recently completed taking data in the S5 science run. Signals from coalescing black-hole binaries will be among the strongest that one hopes to find in the detector data, and data analysts are searching for them by performing matched filtering against template banks of theoretical waveforms. At present data analysts use, or are preparing to use, waveforms calculated by post-Newtonian (PN) methods, principally, the standard Taylor-expanded, effective-one-body (EOB), and BCV [4] waveforms implemented in the LSC Algorithms Library (LAL) [5], although current GW searches do not go beyond second PN order (2PN). The PN waveforms are expected to be reasonably accurate during the slow inspiral of the binaries, but it is not clear how well they can model the merger phase. Ultimately the PN waveforms will be connected to waveforms from fully general-relativistic numerical simulations, which will also model the last orbits, merger, and ringdown.

In the last two years breakthroughs in numerical relativity [6–8] have completed the work of providing the techniques to generate the necessary numerical (NR) waveforms. The nonspinning equal-mass case has been studied in great detail [6–17] and extremely accurate waveforms over many (> 15) cycles are now available [18]. A first comparison of PN and NR equal-mass waveforms was made in [15,19], unequal-mass waveforms were studied in [20–22], and spinning binaries in [23], and the work of producing hybrid NR-PN waveforms has begun [21,22,24,25]. Good agreement has been observed between NR and PN waveforms [15,19,21]; phase disagreements of less than 1 rad up to $\sim$1.5 orbits before merger were seen in [15]. However, until now NR waveforms have not been accurate enough to allow a conclusive comparison with the PN wave amplitude; for example, it was pointed out in [21] that although the disagreement in the amplitude of NR and PN waves was about 10%, this was also the size of the uncertainty in the NR wave amplitude, and it was not possible to conclude what order of PN treatment of the wave amplitude gives the best agreement with fully general-relativistic results.

In this work we systematically compare numerical equal-mass waveforms that include up to 18 cycles before merger with the 3.5PN "TaylorT1" and 3PN "TaylorT3" waveforms implemented in LAL. One could compare with many different varieties of PN waveform, but the T1 and T3 approximants are common choices that are among those proposed for gravitational-wave searches in detector data, and restricting ourselves to only two approximants keeps our analysis and the presentation of our results relatively simple. The region of comparison includes 13 cycles. Considering the amplitude $A(t)$ and phase $\phi(t)$ of our numerical waveforms separately, we find that the accumulated error in $\phi(t)$ is at most 0.25 radians over the frequency range of comparison. These uncertainties are dominated by the finite extraction radii of our waveforms, *not* finite-difference errors. The error in the amplitude $A(t)$ is less than 2% for most of the simulation. We estimate the eccentricity as $e < 0.0016$. We therefore consider these waveforms to be adequately accurate for a detailed comparison with PN results, in particular, to determine the disagreement between NR and PN wave amplitudes.

Numerical simulations are computationally expensive, and mapping the parameter space of binary mergers (including black holes of varying mass ratio and spins) will require huge computer resources. As such, we would prefer to simulate only a small number of orbits before matching with PN results. We find that a simulation of only 4.5 orbits has the same amplitude agreement with the last four cycles of the restricted 3.5PN waveform as the long 18-cycle simulation, and therefore suggest that relatively short numerical simulations are feasible for matching to PN inspiral waves. For an even greater amplitude agreement with PN theory, our results suggest that, using 2.5PN amplitude corrections, at least 5.5 orbits (11 cycles) before merger are necessary.

We also compare the black holes' motion with that calculated by integrating the PN equations of motion [26,27] and find that the PN and NR orbital tracks and frequencies are in excellent agreement until the last three orbits of the binary.

Before describing our analysis in detail, we give a brief summary of our numerical methods in Sec. II and the procedure for generating PN waveforms in Sec. III. In Sec. IV we discuss the simulations we performed and establish the sixth-order convergence of our results, construct Richardson-extrapolated waveforms with error estimates, and extrapolate the finite-extraction-radius waveforms to those measured as $R_{\rm ex} \to \infty$. We also discuss the phase errors in our waveforms and give a consistency check between waves from simulations starting at different initial separations. In Sec. V we directly compare the PN and numerical waveforms.

II. NUMERICAL METHODS AND WAVEFORMS

We performed numerical simulations with the BAM code [13,28], replacing fourth-order accurate derivative operators by sixth-order accurate spatial derivative operators in the bulk as described in [18]. The code starts with black-hole binary puncture initial data [29,30] generated using a pseudospectral code [31], and evolves them with the χ-variant of the moving-puncture [32,33] version of the Baumgarte-Shapiro-Shibata-Nakamura (BSSN) [34,35] formulation of the $3+1$ Einstein evolution equations [36]. The gravitational waves emitted by the binary are calculated from the Newman-Penrose scalar Ψ_4, and the details of our implementation of this procedure are given in [13].

The simulations we performed for this analysis are summarized in Tables I and II. For the configurations with initial separations $D = 10M$, $11M$, $12M$ (denoted by "D10," "D11," and "D12" throughout the paper), simulations were performed at three resolutions, and final results obtained by Richardson extrapolation, as described in Sec. IV. For the $D = 8M$, $9M$ ("D8," "D9") configurations, which are used only for comparison at the end of Sec. V, only one simulation at medium resolution was performed.

TABLE I. Summary of grid setup for numerical simulations.

Grid	$h_{\rm min}$	$h_{\rm max}$	$r_{\rm max}$
D8 simulation			
$\chi_{\eta=2}[5\times 56{:}5\times 112{:}6]$	$M/37.3$	$96/7M$	$775M$
D9 simulation			
$\chi_{\eta=2}[5\times 56{:}5\times 112{:}6]$	$M/37.3$	$96/7M$	$775M$
D10 and D11 simulations			
$\chi_{\eta=2}[5\times 48{:}5\times 96{:}6]$	$M/32.0$	$16M$	$776M$
$\chi_{\eta=2}[5\times 56{:}5\times 112{:}6]$	$M/37.3$	$96/7M$	$775M$
$\chi_{\eta=2}[5\times 64{:}5\times 128{:}6]$	$M/42.7$	$12M$	$774M$
D12 simulations			
$\chi_{\eta=2}[5\times 64{:}5\times 128{:}6]$	$M/42.7$	$12M$	$774M$
$\chi_{\eta=2}[5\times 72{:}5\times 144{:}6]$	$M/48.0$	$32/3M$	$773M$
$\chi_{\eta=2}[5\times 80{:}5\times 160{:}6]$	$M/53.3$	$48/5M$	$773M$

The physical parameters are given in Table II. The initial momenta for low-eccentricity quasicircular inspiral are estimated by the PN method described in [27]. We estimated the eccentricity from the frequency ω_p of the puncture motion, as we did previously for $D = 11M$ simulations in [27], and as also used in [15,19]. Given the puncture motion frequency $\omega_p(t)$ and the frequency of a comparable zero-eccentricity simulation $\omega_c(t)$ (estimated by fitting a fourth-order polynomial in t through the numerical $\omega_p(t)$, as suggested in [15]), the eccentricity is estimated by finding extrema in the function $(\omega_p(t) - \omega_c(t))/(2\omega_c(t))$. The uncertainty in the eccentricity estimate is about 2×10^{-4} [27]. A simulation with initial $D = 12M$ but using "quasicircular orbit" parameters (as discussed further in Sec. V C) has an eccentricity of $e \approx 0.008$, i.e., 5 times larger than the eccentricity of the D12 simulation.

TABLE II. Physical parameters for the moving-puncture simulations: the coordinate separation, D, the mass parameters in the puncture data construction, m_i, and the magnitude of the momenta p_x and p_y. The punctures are placed on the y-axis, and all quantities are scaled with respect to the total initial black-hole mass, $M = 1$. The momenta are based on those described in [27], and produce quasicircular inspiral with minimal eccentricity. The estimated eccentricity e is also given, as described in the text. The time t_A is the time (in M) when the wave amplitude reaches a maximum at extraction radius $R_{\rm ex} = 90M$.

	D	m_i	p_x	$p_y\ (\times 10^{-3})$	e	t_A
D8	8.0	0.482 40	0.112 35	2.0883	0.0025	458
D9	9.0	0.484 36	0.103 37	1.4019	0.0022	673
D10	10.0	0.485 93	0.096 107	0.980 376	0.0022	981
D11	11.0	0.487 21	0.090 099	0.709 412	0.0020	1390
D12	12.0	0.488 28	0.085 035	0.537 285	0.0016	1940

For comparison between PN and numerical results, we must make clear what we mean by the individual black-hole masses M_1 and M_2, and the total mass M. The mass of each black hole, M_i, is specified in terms of the Arnowitt-Deser-Misner (ADM) mass at each puncture. This corresponds to the mass at the other asymptotically flat end, and has been found to equal numerically the apparent-horizon mass [37], which for nonspinning black holes is related to the area of the horizon A_i by

$$M_i = \sqrt{\frac{A_i}{16\pi}}. \tag{1}$$

We assume that this mass is the same as the mass used in post-Newtonian formulas. Rather than try to quantify the accuracy of this assumption, we make the following argument, which we consider to be a more practical approach. Our assumption is rigorously true only in the limit where the black holes are infinitely far apart and stationary. As such we consider any error in this assumption as part of the error due to starting the simulation at a finite separation. Since there is no invariant measure of quasilocal mass in general relativity, this error is present in some form in all numerical simulations. In practice one could rescale the total mass to optimize the phase and amplitude agreement with post-Newtonian calculations, but in the present work we retain the assumption that the horizon mass and PN masses can be equated at the beginning of the simulation. This provides an overall scale $M = M_1 + M_2$ for both numerical and post-Newtonian waveforms, and is crucial for comparison and matching.

Let us discuss some other possible sources of error related to the masses and spins of the black holes in our numerical simulations.

The initial data contain "junk" radiation that quickly leaves the system. Some of this radiation may fall into the black holes and alter their masses. To estimate this effect, we refer to the initial-data studies of Cook and York [38,39], who estimated the maximum radiation content of single boosted Bowen-York black-hole initial-data sets (recall that a single boosted Schwarzschild black-hole spacetime will not contain any gravitational radiation). An estimate based on their data suggests that the spacetime of a Bowen-York black hole with $P_i/M_i \approx 0.17$ (which is the case for the D12 simulations) has a maximum gravitational-wave energy content of 0.01% of the mass. In our simulations, the radiated energy from the junk radiation is at least 0.005% of the initial mass. Therefore we estimate that at most 0.005% of the mass fell back into the black hole. An error in our estimate of the total mass of 0.005% would lead to a phase error in a $2000M$ simulation of $0.1M$. We calculate (see Sec. IV) a numerical uncertainty in the merger time of $0.4M$, making any effect due to junk radiation falling into the black holes lower than our numerical uncertainty, and therefore not detectable at our level of accuracy.

A further possible issue with the mass is that it may drift due to numerical error over the course of the simulation. However, since we see clean sixth-order convergence in the time when the gravitational wave amplitude reaches a maximum, we expect that any mass drift either also converges away at sixth order, or is well below the error due to other numerical effects.

Finally, one may worry that the black holes pick up spin during their evolution. This effect has already been studied by Campanelli, *et. al.* [40]. We do not attempt to measure this effect in our simulations, for the following reason: we are comparing numerical and PN waveforms of binaries that initially consist of nonspinning black holes. In the PN approach we use, the black holes remain nonspinning. Any spin that they acquire in full general relativity will therefore contribute to the disagreement between PN and NR waveforms. It is that difference in the waveforms that we are interested in measuring. More detailed investigation of the physical properties of nonspinning binaries is beyond the scope of this study.

III. POST-NEWTONIAN WAVEFORMS

Binary inspiral waveforms can be constructed by a variety of means. We choose to compare our numerical waveforms with PN waveforms that are proposed for future searches for gravitational-wave signals from black-hole binary coalescence, namely, the Taylor-expanded or EOB-resummed waveforms implemented in the LSC Applications Library (LAL) [5,41,42]. In particular, we compare with the 3.5PN Taylor T1 waves, with a version of the code[1] that includes modifications to the flux coefficients given in the erratum to [41,42]. In the Taylor T1 approach ordinary differential equations are solved numerically to give the phase of the wave, and the amplitude is estimated by the quadrupole contribution, which is proportional to $x = (M\omega/2)^{2/3}$, where ω is the gravitational-wave frequency, and $\omega/2$ is assumed to be the orbital frequency of the binary. This treatment of the amplitude yields "restricted" PN waveforms. In Sec. V we also compare with a 2.5PN treatment of the amplitude [43], which includes terms up to $x^{7/2}$.

To check the consistency of our comparison, we also compare with the "Taylor T3" PN approximant [44,45], which consists of an analytic expression for the gravitational-wave phase as a function of the variable $\tau = \eta(t - t_c)/(5M)$, where t_c is the "coalescence time" of the binary, M is the total mass, and $\eta = M_1 M_2/M^2$ is the symmetric mass ratio. The T3 approximant for the phase also contains a free phase constant, ϕ_0. The coalescence time t_c and phase constant ϕ_0 can be chosen to line up the phase and frequency of a T3 PN waveform with a NR

[1]We used a version of LAL consistent with a cvs version dating from July 11, 2007; earlier versions contain errors in the TaylorT1 implementation.

waveform at a given time. We use the TaylorT3 approximant up to 3PN order, because the 3.5PN term contains an unphysical turning point long before the merger, which was already noted in the PN comparisons made in [15,19].

The LAL code that we use, `LALInspiralTest`, produces h_+ and/or h_- as a function of time. From this function we can compute the real part of $\Psi_{4,(l=2,m=2)}$ by differentiating twice with respect to time. We choose $\Psi_{4,22}$ as the quantity to compare between NR and PN waveforms for two reasons: (1) we can compute the PN $h_{+,-}$ with arbitrarily small discretization error, and thus expect that its derivatives will be more accurate than computing $h_{+,-}$ by integration of the NR $\Psi_{4,22}$; (2) integration of $\Psi_{4,22}$ requires estimating two constants of integration, which further complicates the procedure. In short, it should be equivalent to compare waveforms using $h_{+,-}$ and $\Psi_{4,22}$, and we choose $\Psi_{4,22}$ because it is more straightforward.

To generate a PN waveform we must choose the masses of the two bodies, and a range of frequencies that we want the waveform to cover. The masses are specified in units of solar mass. To produce the quantity $r\Psi_{4,22}$ that we wish to compare with numerical data, the time is rescaled to be in units of M by multiplying by the factor c/M, where we chose $M = 2M_\odot = 2953.25$ m (although the choice of masses is arbitrary) and the speed of light is $c = 2.9979 \times 10^8$ m/s. The PN wave strain is then differentiated twice with respect to time, and the amplitude is scaled by the factor $\sqrt{16\pi/5}$ to give the coefficient of the $l = 2$, $m = 2$ mode.

IV. NUMERICAL SIMULATIONS: ACCURACY AND CONSISTENCY

In this section we describe our procedure for producing the most accurate waveform possible from our numerical data. This consists of taking waveforms calculated at five extraction radii from simulations performed at three resolutions, and (1) Richardson extrapolating these waveforms with respect to numerical resolution to produce accurate waveforms at each of the five extraction radii, and then (2) extrapolating with respect to extraction radius to estimate the signal that would be calculated as $R_{\rm ex} \to \infty$.

In [18] we described the use of sixth-order accurate spatial finite differencing in the bulk in BAM, introduced to increase the overall accuracy and, in particular, reduce the phase error in long evolutions. We found that $\mathrm{Re}(r\Psi_4)_{22}$, as directly computed by the code, was sixth-order convergent only up to about $100M$ before merger. However, if we separate the waveform into its amplitude and frequency as

$$r\Psi_4 = A(\phi(t))e^{i\phi(t)}, \tag{2}$$

and examine separately $\phi(t)$ and $A(\phi)$, then the phase shows reasonably clean sixth-order convergence throughout the evolution (with a small "blip" around the merger time), and the amplitude computed as a function of the phase angle shows good convergence with far lower errors than when we consider simply $A(t)$. This is because $A(t)$ includes errors from the phase as well as the amplitude measurement; considering $A(\phi)$ allows us to isolate the phase errors from the amplitude errors. With this phase/amplitude split we are able to perform Richardson extrapolation and reconstruct a more accurate waveform and calculate an error estimate. More details about the convergence properties of these simulations can be found in [18].

In order to be as clear as possible about this procedure, we will outline in detail the steps we followed to produce the D12 waveform that will form the basis of our comparison with PN waveforms.

We perform three simulations with the grid configuration (following the notation in [13]) $\chi_{\eta=2}[5 \times N{:}5 \times 2N{:}6]$, where $N = 64$, 72, 80 for the D12 runs. The grid resolutions on the finest inner box are $M/42.67$, $M/48$, and $M/53.33$, and the resolutions on the coarsest outer levels are $12M$, $10.67M$, and $9.6M$, placing the outer boundary at about $775M$. The wave extraction is performed at resolutions $1.5M$, $1.33M$, and $1.2M$. The grid setup is summarized in Table I, which also provides the grid details for the D8, D9, D10, and D11 simulations.

In each simulation, waves are extracted at radii $R_{\rm ex} =$ 40, 50, 60, 80, and $90M$. Figure 1 shows that the phase displays good sixth-order convergence over the course of the entire evolution. In order to disentangle the error in the phase from that in the amplitude, we now consider the amplitude as a function of *phase*, rather than time, $A(\phi)$, and show in Fig. 2 that this function is also sixth-order convergent. For comparison Fig. 3 shows a convergence plot of the amplitude as a function of time, $A(t)$, with no adjustments made for the phase. We see that $A(t)$ is sixth-order convergent, but the differences are almost a factor of 10 larger than they are for $A(\phi)$; this demonstrates the utility of considering $A(\phi)$ instead of $A(t)$.

The figures show the amplitude and phase from the waves extracted at $R_{\rm ex} = 90M$, but similar properties are seen at all five extraction radii. Note that in these figures, and in all other relevant figures in this paper, the horizontal axis displays the time from the numerical code. For example, in Fig. 1 the wave phase shown at $t = 1000M$ is the phase of the wave measured at the extraction sphere at $R_{\rm ex} = 90M$ at code time $t = 1000M$. In subsequent plots, when some time shifting has been applied, we indicate how this relates to the code time as displayed in any figures.

Given the clean sixth-order convergence of $A(\phi)$ and $\phi(t)$, we apply Richardson extrapolation to $A(\phi)$ and $\phi(t)$ at each extraction radius. Since we have results at three resolutions, we are also able to compute an error estimate for the Richardson-extrapolated results. If a function in the continuum limit is f, and a numerical calculation of it, $\tilde{f}$, is sixth-order accurate, then we can write

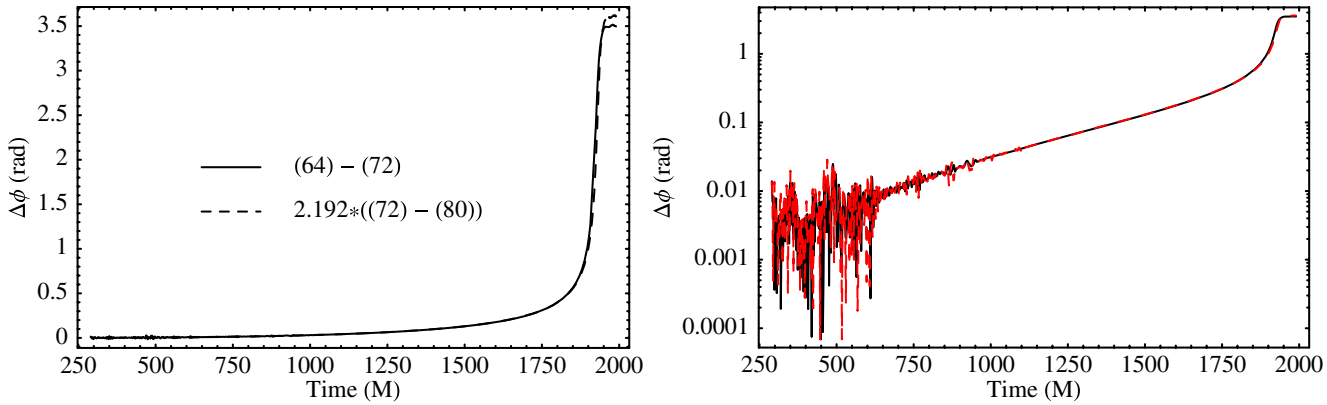

FIG. 1 (color online). Convergence of the phase $\phi(t)$. Differences between simulations with $N = 64, 72, 80$ (see Table I) are scaled assuming sixth-order convergence. The convergence of the phase is shown as both a standard and a logarithmic plot, to demonstrate that good sixth-order convergence is seen throughout the simulation, except after merger, when there is a slight drop in convergence. In the logarithmic plot the solid and dashed lines are so close as to be almost indistinguishable.

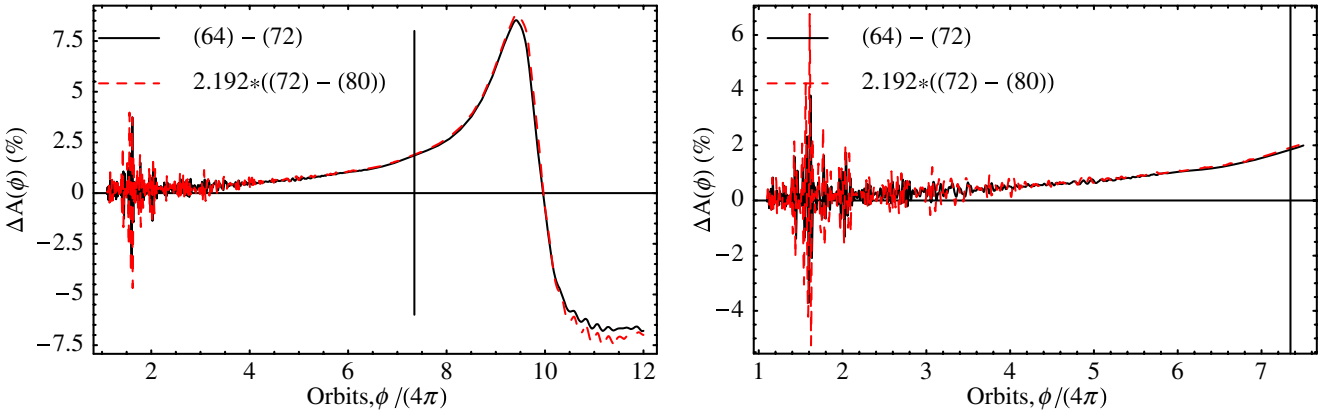

FIG. 2 (color online). Convergence of the amplitude $A(\phi)$. Differences between simulations with $N = 64, 72, 80$ (see Table I) are scaled assuming sixth-order convergence. The x-axis shows $\phi/(4\pi)$, which gives a rough estimate of the number of orbits the system has completed (at least before merger). The phase ϕ is chosen to be in the interval $[-\pi, \pi]$ at $t = 0$. The convergence of the amplitude is shown in terms of relative (percentage) errors, to allow easier comparison with later results. A vertical line indicates the point at which we end our PN comparison in Sec. V. The plot on the right zooms into the region that will be used for PN comparison.

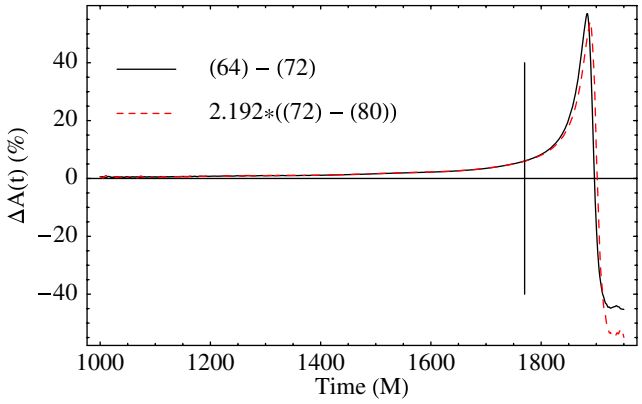

FIG. 3 (color online). Same as Fig. 2, but using $A(t)$ instead of $A(\phi)$. We see that the differences are far larger than for $A(\phi)$; the maximum difference is now around 60%, while it was only 8% when we considered $A(\phi)$.

$$\tilde{f} = f + a_1 h^6 + a_2 h^7 + O(h^8), \tag{3}$$

where h is the grid spacing. With results at two resolutions, Richardson extrapolation involves calculating the coefficient a_1 and removing the sixth-order error to give a result that is seventh-order accurate. With results at three resolutions, we may also calculate a_2, and taking the difference between estimates of the true solution f using only a_1 or both a_1 and a_2, we can estimate the error in the Richardson-extrapolated result. These errors are shown in Fig. 4 for the portion of the simulation that will be compared with PN waveforms. We see that for $t > 500M$ the uncertainty in $\phi(t)$ is less than 0.01 radians, and the uncertainty in $A(\phi)$ is less than 0.5%. At earlier times the uncertainties grow by up to a factor of 10, due to noise in the data.

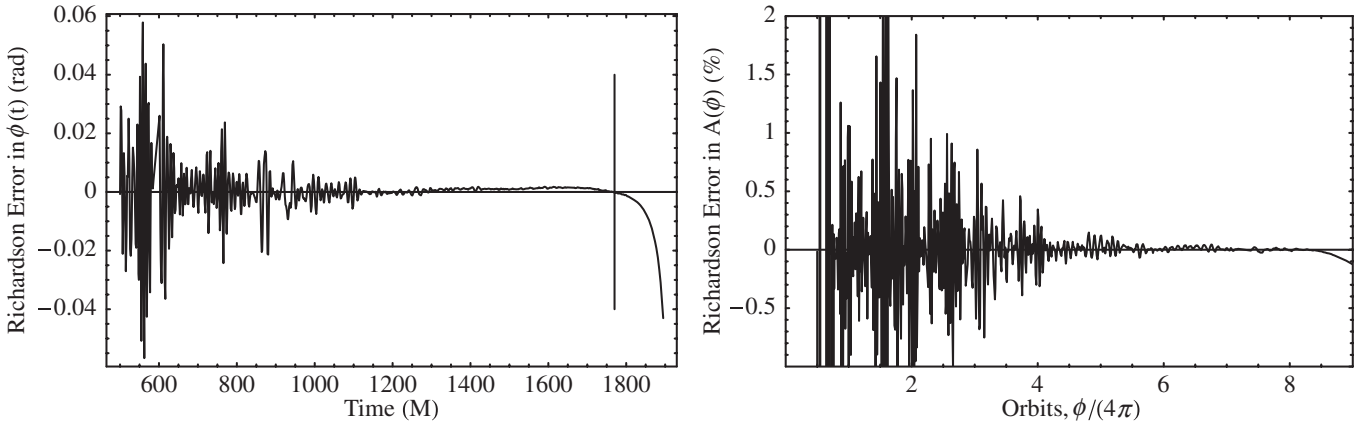

FIG. 4. Error in the Richardson-extrapolated functions $\phi(t)$ and $A(\phi)$. For the range of the simulations that will be compared with PN waveforms, the uncertainty in $\phi(t)$ is below 0.01 radians at most times, and the uncertainty in the amplitude is less than 0.5%. At earlier times $t < 500M$, which are also nominally included in the PN comparison), these plots are dominated by noise and the uncertainty grows by a factor of 10.

We now have amplitude and phase functions $A(\phi)$ and $\phi(t)$ for each of the five extraction radii, and wish to extrapolate to $R_{\rm ex} \to \infty$.

We first deal with $A(\phi)$. Since we are looking at the amplitude as a function of phase, rather than time, the amplitudes measured at each extraction radius are already in phase; there is no need to "line them up," as would be necessary if we looked at $A(t)$. We find that the value of the five amplitude functions is approximated well by a quadratic function in extraction radius, i.e.,

$$A(\phi, R_{\rm ex}) = A_\infty(\phi) + \frac{k(\phi)}{R_{\rm ex}^2} + O\left(\frac{1}{R_{ex}^3}\right). \qquad (4)$$

In other words, the wave amplitude error falls off as the square of the extraction radius. A simple curve fit (performed at each phase ϕ) allows us to construct $A_\infty(\phi)$. Including the next fall-off term, $1/R_{\rm ex}^3$, allows us to also estimate the uncertainty in the extrapolation, analogous to the method of error estimate in the Richardson extrapolation of the discretization error. Note that although one would expect the error to fall off as $1/R_{\rm ex}$, our results suggest that the quadratic falloff dominates; this has also been observed in simulations of a particle orbiting a Kerr black hole [46]. The quadratic falloff in the amplitude error is demonstrated in Fig. 5. The resulting relative error estimate as a function of ϕ is shown in Fig. 6, and as a result of this plot we estimate the uncertainty in $A(\phi)$ due to extrapolation to $R_{\rm ex} \to \infty$ as about 2%. This dominates the uncertainty from Richardson extrapolation ($< 0.5\%$), so we also estimate the overall uncertainty in $A(\phi)$ as about 2%.

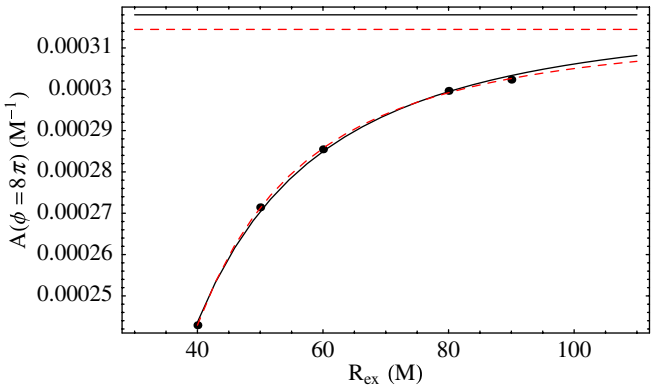

FIG. 5 (color online). The wave amplitude A as a function of extraction radius $R_{\rm ex}$, at $\phi = 8\pi$, which corresponds to $t \approx 715M$ for the wave extracted at $R_{\rm ex} = 90M$. The solid line shows a curve fit of the form (4). The dashed line shows a curve fit with an extra $1/R_{\rm ex}^3$ term. The horizontal solid and dashed lines show the corresponding $R_{\rm ex} \to \infty$ limits of the two curve fits; our uncertainty estimate in the extrapolation of the amplitude comprises the difference of these two values.

We now turn to the phase, $\phi(t)$. To a first approximation we expect that the difference in the phase measured at two extraction spheres will be a constant. However, the proper

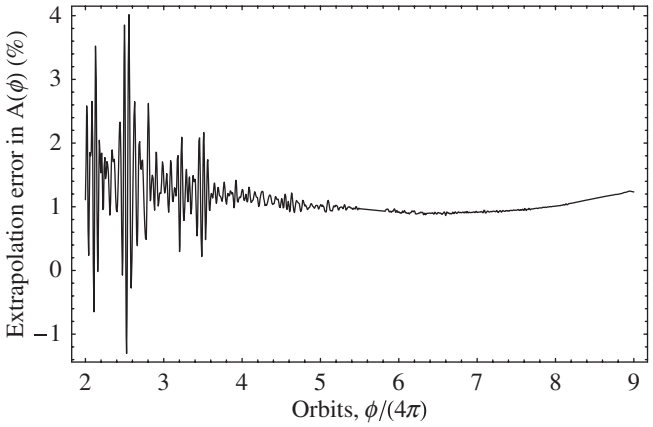

FIG. 6. Error in the $R_{\rm ex} \to \infty$ extrapolated function $A(\phi)$. For the range of the simulations that will be compared with PN waveforms, the uncertainty in the amplitude is less than 2%.

distance between each extraction sphere may drift due to gauge effects. We have already seen in evolutions of the Schwarzschild spacetime that the coordinate location of the horizon drifts depending on the value of the η parameter in the $\tilde{\Gamma}$-driver shift evolution equation (see Fig. 4 in [13]), and effects related to η have also been observed and studied in [47,48]; and it is quite possible that there are other gauge effects that we are not aware of.

We have attempted to extrapolate the phase to $R_{\rm ex} \to \infty$ by lining up the phase at a given time, and then observing, at other times, the deviations in the phase at different extraction radii. These deviations decrease as $R_{\rm ex}$ increases, and the falloff can be reasonably well modeled by a polynomial in $1/R_{\rm ex}$, and far better by a polynomial in $1/R_{\rm ex}$ and $1/R_{\rm ex}^2$. However, we do not find the limit as $R_{\rm ex} \to \infty$ to be very robust—the results vary depending on the choice of the time when the phases are lined up. (Obvious choices for this time are when the gravitational-wave amplitude reaches a maximum, near merger, or the time at which the GW frequency $M\omega$ equals one of the matching values that will be used in our PN comparison below.) As such, we do not extrapolate the phase. We instead use the phase at the largest extraction radius, $R_{\rm ex} = 90M$ (which we expect to be the most accurate) and use the phase extrapolation procedure to estimate the uncertainty in the phase, which we give as 0.25 radians.

An alternative indication of the accumulated phase error of the numerical simulations is given by the time when the amplitude of the gravitational-wave signal reaches a maximum. This time is also seen to be sixth-order convergent, and a similar Richardson-extrapolation error estimate as performed above gives an uncertainty of $0.4M$ in the "length" of the simulation.

We are now able to construct a final waveform,

$$\mathrm{Re}\,(r\Psi_{4,22}(t)) = A_\infty(\phi_{90}(t))\cos(\phi_{90}(t) - \delta), \quad (5)$$

$$\mathrm{Im}\,(r\Psi_{4,22}(t)) = A_\infty(\phi_{90}(t))\sin(\phi_{90}(t) - \delta), \quad (6)$$

where δ is an arbitrary phase shift, which we will apply later when comparing with PN waveforms. The uncertainty in the wave amplitude is about 2%, and the accumulated phase error over the time range we will consider is about 0.25 radians. The time-shifting process described earlier means that the extrapolated waveform is measured at an effective extraction sphere with $R_{\rm ex} = 90M$, i.e., our extrapolated waveform gives the wave amplitude that would be measured at infinity, but at a time roughly $90M$ after the

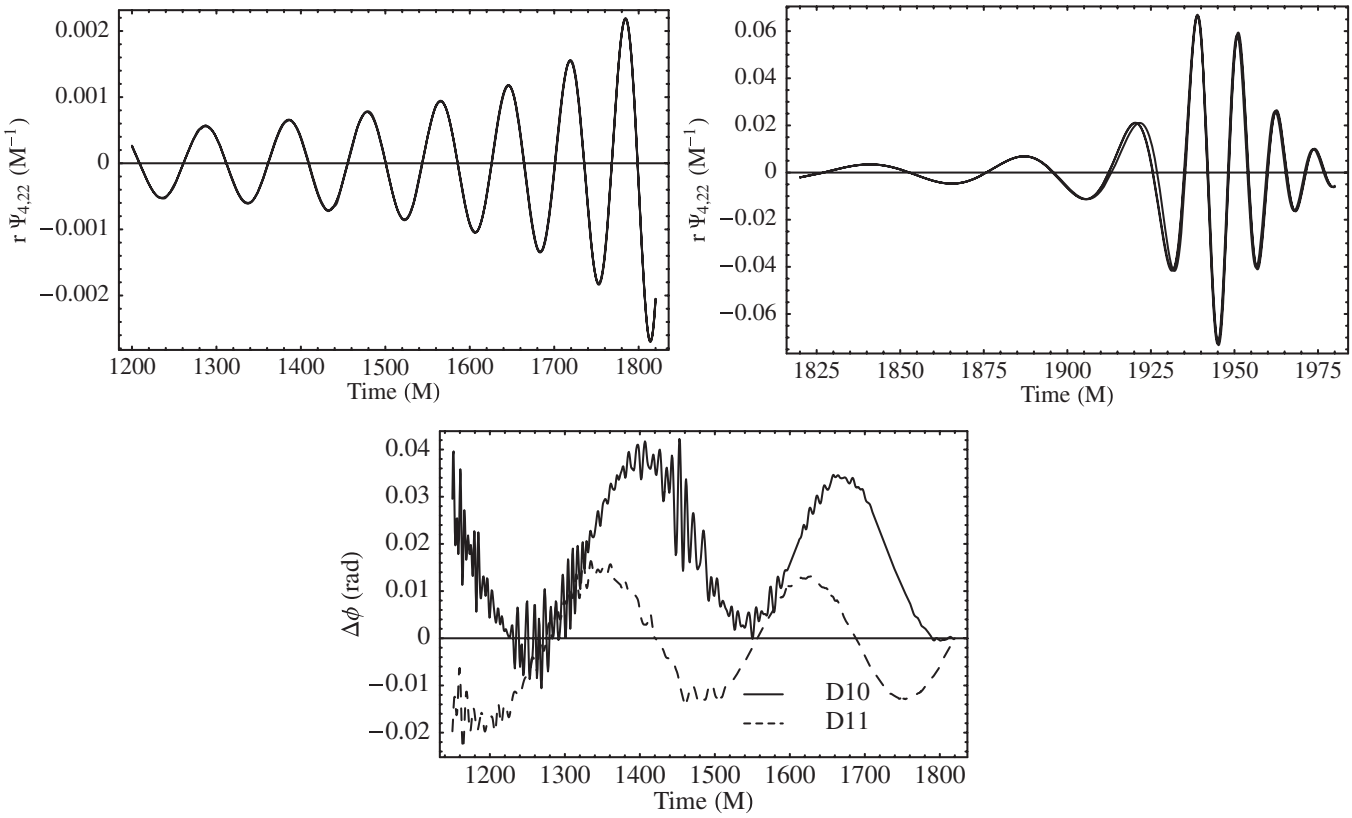

FIG. 7. Final waveforms from the D10, D11, and D12 runs, produced by the method discussed in the text and shifted in time so that their amplitude maxima occur at the same time. The three lines are not individually labeled; the main point is that their differences are almost indistinguishable, except in the last cycle before merger; see text. The phase disagreement with the D12 simulation is shown in the lower panel.

wave was emitted from the binary system. Since we do not make direct comparisons between quantities calculated from the gravitational waves and quantities calculated from the puncture motion, it is not necessary to know this ''wave travel time'' precisely. Although not used here, one could estimate this time using the method suggested in [49].

The same procedure is applied to the simulations D10 and D11. With a suitable time shift applied so that the wave amplitude maximum occurs at the same time, the extrapolated waveforms from the three simulations are shown in Fig. 7. The waveforms lie almost perfectly on top of each other, except in the last cycle before merger. It is at this time that we see a ''glitch'' in the clean convergence of the phase $\phi(t)$. However, for comparison with 3.5PN waveforms we will only be interested in the waveform before $t \approx 1770M$. In order to quantify the level of agreement between the D10, D11, and D12 waveforms, we also show in the lower panel of Fig. 7 the accumulated phase error between $t = 1200M$ and $t = 1800M$ (where t is the code time of the D12 simulation). We see that the phase errors average to below 0.03 radians, consistent with the numerical error estimate in Fig. 4.

V. COMPARISON

Given the PN and NR waveforms discussed in Secs. III and IV, we are now in a position to compare them. Most of our comparisons are matched with respect to the gravitational-wave frequency, which we define as $\omega = d\phi(t)/dt$, and we always deal with the dimensionless quantity $M\omega$. We compare NR waveforms with a 3.5PN TaylorT1 waveform that was terminated at a gravitational-wave frequency $M\omega = 0.120$, but we will only use it up to a cutoff frequency of $M\omega_0 = 0.1$; since the growth in phase error in the 3.5PN waveform becomes dramatic at late times (see, for example, Fig. 17 in [21]), the smaller the choice of cutoff frequency the better. Figure 8 shows the numerical D12 $r\Psi_{4,22}$ overlaid with the 3.5PN TaylorT1 version computed from output from the LAL code. The figure starts at $t = 340M$, after the binary has completed one orbit; this allows time for noise due to the junk radiation in the initial data to leave the system. The agreement between the PN and numerical waveforms appears to be excellent. A similar plot (for h_+) is shown in Fig. 1 of [15].

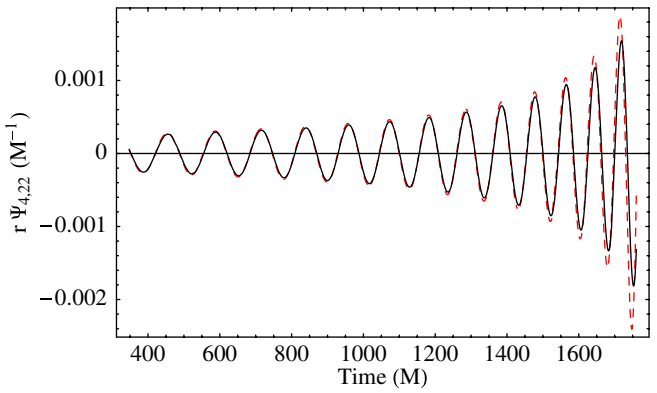

FIG. 8 (color online). Numerical (solid line) and TaylorT1 3.5PN (dashed line) waveforms $r\Psi_{4,22}$ for equal-mass inspiral.

The NR and PN waveforms shown in Fig. 8 were ''lined up'' by first identifying the time at which both waveforms had a given frequency $M\omega_0$. An appropriate phase shift δ was then applied to the numerical waveform to line up the PN and NR phases. The choice of $M\omega_0$ can have a dramatic effect on the quality of the phase agreement between the PN and NR waveforms. Figure 8 was produced by matching at the beginning of the comparison region, at $M\omega = 0.0455$, which gives a far better phase match, as we will discuss below.

We will now discuss this subtle feature of the matching process in more detail, before we make any conclusions about the agreement between NR and 3.5PN TaylorT1 waveforms.

A. Phase and frequency

The wave frequency $M\omega$ calculated from the NR waves is typically very noisy at early times, but becomes much smoother near merger, when the value is higher. To allow a matching at any time in the window of comparison, we fit a polynomial in time through the numerical frequency to produce a smoother function. The curve fit is based on the form of the frequency evolution in the TaylorT3 approach, i.e., a polynomial in $(t - t_c)$, where t_c is a crude estimate of the merger time (its specific value does not strongly affect the accuracy of the fit; we used $t_c = 1927M$), and the powers of $(t - t_c)$ that are included are $\{-3/8, -5/8, -3/4, -7/8, -1, -9/8\}$. The use of a curve fit introduces yet another source of error in our numerical phase, particularly at early times, which is difficult to assess. However, the analyses below were repeated with different fitting functions (by keeping or removing the last term in the fit, or varying t_c), and all changes in the phase results were below the stated numerical phase uncertainty of 0.25 radians. Nonetheless, we tend to consider any matching done at late times to be more reliable than that done at early times.

On the other hand, we expect the PN phase to be most accurate at early times—in principle, we should be able to obtain arbitrary accuracy in the post-Newtonian expressions by going to sufficiently early times. For that reason we first choose to line up the frequencies at $t = 347.4M$ in code time (recalling that this is the time when the wave reaches the extraction sphere at $R_{\rm ex} = 90M$), when $M\omega = 0.0455$. We are then free to make a constant phase shift δ to align the phase of the waves; again aligned at $t = 347.4M$ with $\delta = 1.367\pi$. The agreement between the NR and 3.5PN wave frequencies as a function of time is shown in Fig. 9. As can be seen in the right-hand panel of Fig. 9, the PN and NR frequencies remain close up to around

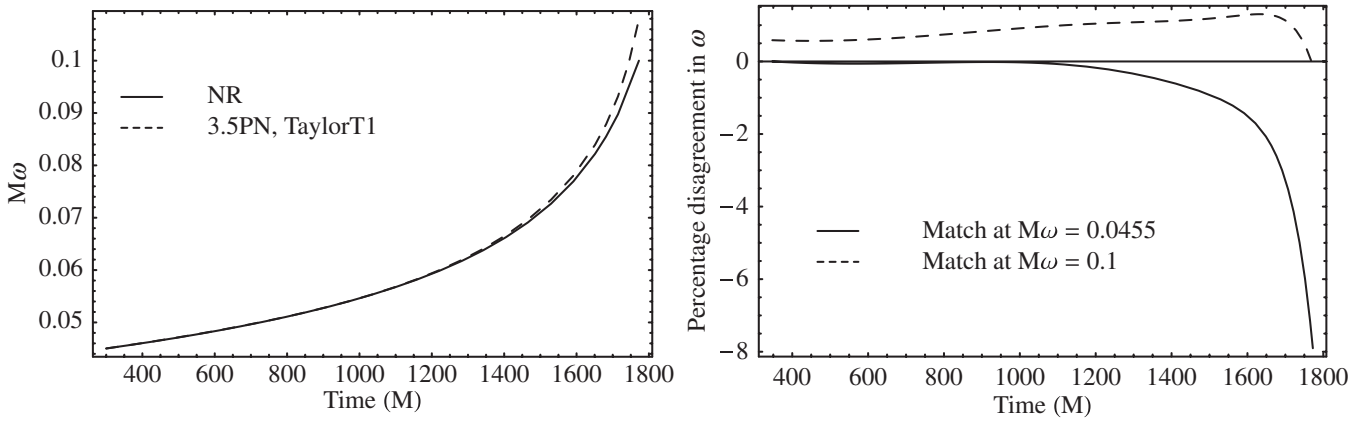

FIG. 9. The wave frequency ω as a function of time for the D12 NR and TaylorT1 3.5PN waveforms. The frequencies agree at $t = 347.4M$, when $M\omega = 0.0455$. The percentage disagreement between the two is shown in the panel on the right. Also shown is the frequency disagreement when matching is done at $M\omega = 0.1$, $t = 1772M$.

$t = 1000M$, and then drift apart and finally diverge. Also shown (with a dashed curve) is the result of matching at the *end* of the comparison region (at $t = 1772M$, with $M\omega_0 = 0.1$, $\delta = 1.067\pi$).

The corresponding results for the phase disagreement are shown in Fig. 10. Also shown is the phase disagreement between the NR waveform and a waveform produced using the TaylorT3 approximant. In order to line up the phase and frequency of the T3 waveform, we choose an appropriate coalescence time t_c and phase constant ϕ_0.

Figure 10 demonstrates that the different choices of matching frequency can give entirely different impressions of the relative merits of the T1 and T3 approximants: when the waves are matched at $t = 1772M$, the accumulated phase disagreement between the T3 approximant and numerical results is about 0.1 radians. When the matching is done at $t = 347.4M$, the accumulated T3/NR phase disagreement is almost 1 rad. In both cases the T1/NR disagreement is comparable, although this is purely an accident of the matching frequencies that were chosen. It should be clear from the right-hand panel of Fig. 10 that if we cut off the comparison at $t = 1000M$, the T1/NR accumulated phase disagreement will be very small. Similarly, for matching purposes, one could optimize the matching time to give the smallest phase disagreement—for the T1 waveforms, we can, for example, match at $M\omega \approx 0.075$ and achieve a phase agreement within numerical uncertainty.

We repeat that for the purposes of comparing PN and NR phases, the match at $M\omega = 0.1$, when the numerical data is relatively free of noise, is the most trustworthy. The matches at earlier times are less accurate and mainly serve to illustrate the general trend in the disagreement between PN and NR phases: the frequency disagreement changes sign (as shown in Fig. 9), and, depending on the approximant used and the chosen matching time and frequency, the phase disagreement may behave as in the T3/NR curve in the left panel of Fig. 10 or the T1/NR curve in the right

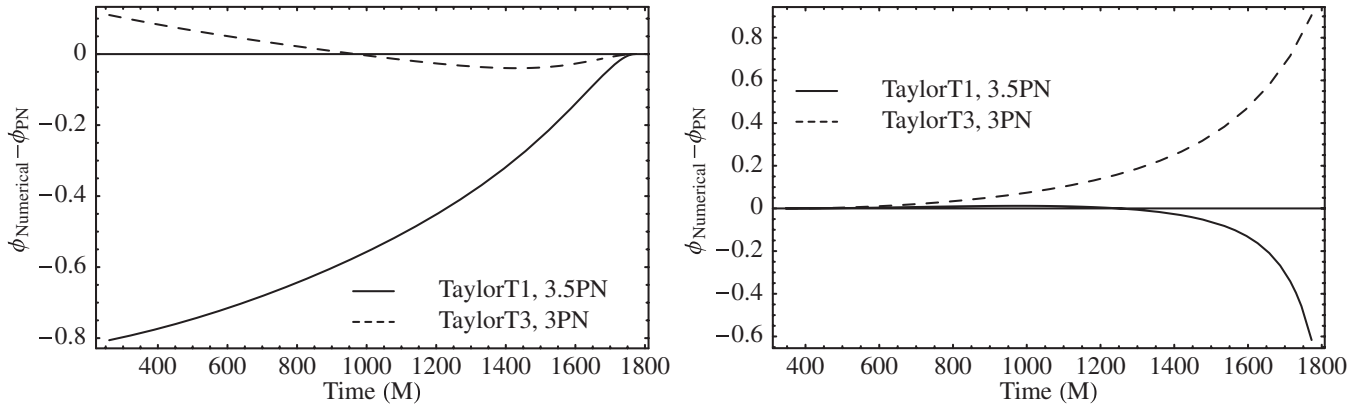

FIG. 10. The disagreement in the phase between NR waveforms and PN waveforms constructed with the TaylorT1 and TaylorT3 approximants. In the left plot the phase and frequency are matched at $t = 1772M$, $M\omega = 0.1$. In the right plot they are matched at $t = 347.4M$, $M\omega = 0.0455$. We see that the relative merits of the two approximants can appear quite different depending on the matching time.

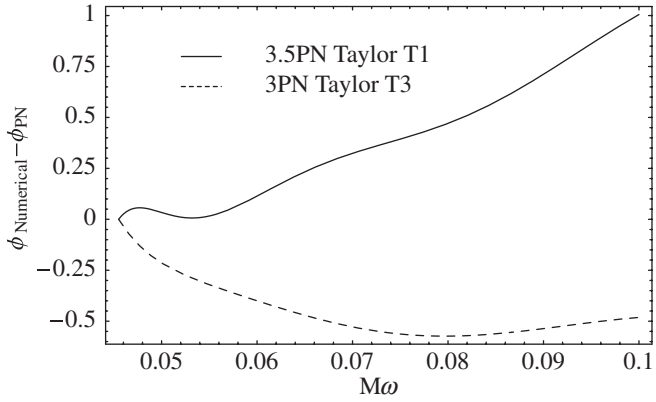

FIG. 11. The disagreement in the phase between NR waveforms and PN waveforms constructed with the TaylorT1 and TaylorT3 approximants, but now shown as a function of GW frequency $M\omega$.

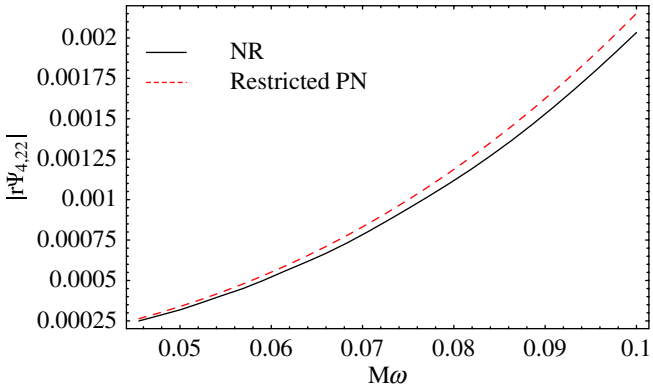

FIG. 12 (color online). NR and restricted PN amplitudes of $r\Psi_{4,22}$. The amplitudes are plotted versus $M\omega$, for which the restricted PN amplitude is unique, i.e., independent of the choice of approximant for the phase evolution.

panel, and exhibit a local maximum, which allows us to optimize the phase disagreement.

We may produce yet another picture of how T1 and T3 behave by plotting the phase disagreement versus the wave frequency $M\omega$, as done in [15]. This is shown in Fig. 11, which now suggests that T3 behaves far better than T1.

What are we to conclude, then, about the phase agreement between NR and T1 or T3 PN waveforms? Because of a turning point in the evolution of the frequency disagreement, we are left with a great deal of freedom about how to match the frequency and phase. We find, in the frequency range that we consider, that the minimum accumulated phase disagreement that we can achieve is about 0.2 (or 0.15) radians using either the T1 (or T3) approximants (see Fig. 10). By contrast, the maximum disagreement between the NR and PN phases over the comparison region is about 1 rad, although since this results from a matching at early times, and the phase disagreement is diverging at the end of the comparison region, this value has a large uncertainty.

When matching NR and PN results to produce hybrid waveforms (as performed in, for example, [24,25]), we naturally choose to match in such a way that the phase disagreement is minimized. We could easily have found that the PN phase evolution disagreed so badly with the NR phase evolution that it was not possible to achieve an accumulated phase disagreement of less than, for example, 1 rad. However, the minimum accumulated phase disagreement that we can achieve is about 0.2 radians, which is also within the phase uncertainty of the numerical waveforms.

We therefore conclude that we can match the phase within the numerical uncertainty over the frequency range we have considered ($M\omega = 0.0455$ up to $M\omega = 0.1$), and that the accumulated PN and NR phase disagreement has an upper bound of roughly 1 rad. We expect that matching at even earlier times (using longer simulations) would make the matching clearer, although this will also require more accurate simulations and larger radiation extraction radii to resolve the lower-frequency, lower-amplitude waves.

B. Amplitude

We now turn to the amplitude.

Figure 12 shows the amplitude of $r\Psi_{4,22}$ from NR and restricted PN waves, plotted as a function of GW frequency $M\omega$, so that the choice of PN approximant does not affect the result. The amplitude of the restricted 3.5PN wave is larger than that for the NR wave. Figure 13 shows the percentage disagreement between the restricted PN and NR wave amplitudes over the same frequency range. The

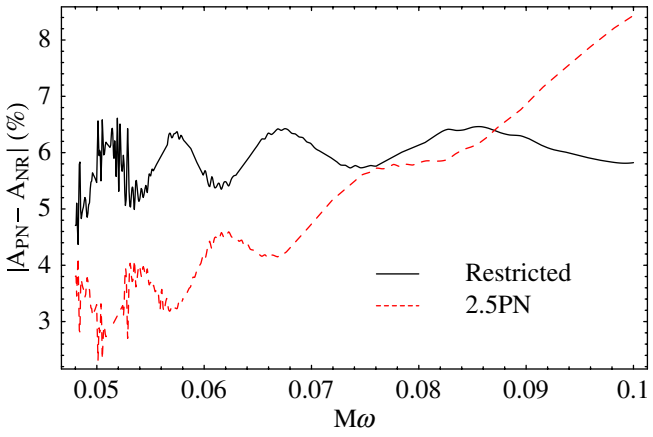

FIG. 13 (color online). Percentage disagreement between the NR wave amplitude and that of the PN waves with the restricted (quadrupole) and 2.5PN amplitude treatments. At low frequencies the disagreement between the 2.5PN and NR amplitudes is close to the uncertainty in the numerical value. The figure gives the absolute value of the disagreement: for reference, $A_{\rm PN,\ restricted} > A_{\rm NR}$ and $A_{\rm 2.5PN} < A_{\rm NR}$.

disagreement is of the order of 6%. Since the uncertainty in the NR wave amplitude is below 2%, at least for $M\omega > 0.05$, we cannot ascribe this disagreement entirely to numerical error. If we assume that the NR wave more closely models the correct physics of the binary system, then the restricted PN (quadrupole) amplitude overestimates the amplitude by between 4% and 8% in this frequency range.

So far we have compared our NR waveforms with *restricted* 3.5PN waveforms, meaning that the amplitude in the gravitational-wave strain is proportional to $x = (M\omega/2)^{2/3}$. (The factor of 2 signifies that x deals with the frequency of the black holes' motion, not the frequency of the waves; the two frequencies are assumed to be related by a factor of 2.) If we move beyond restricted waveforms, and model the amplitude up to 2.5PN order (i.e., with terms up to $x^{7/2}$) [15,43], we find greater disagreement at higher frequencies, but at low frequencies the 2.5PN amplitude shows better agreement with the NR amplitude. The 2.5PN amplitude disagreement at $M\omega = 0.0455$ is between 1% and 5%; the PN and NR amplitude disagreement is now close to the numerical uncertainty. This is also shown in Fig. 13.

As we have said, the amplitude disagreement between the NR and restricted PN amplitudes is roughly constant over the frequency range $M\omega = 0.05$ to $M\omega = 0.1$. This suggests that if we are content with these levels of error when matching numerical and PN waveforms, the large number of cycles in the D12 simulation is not necessary. A combined PN-NR waveform could be produced by applying a scale factor, as is done using different approaches in [21,24,25], and clearly only a few cycles shared by the NR and 3.5PN waveforms are needed to determine the scale factor. We may now ask: can we get away with a numerical simulation that starts at, for example, $D = 9M$, and yields a waveform that (neglecting the first orbit) shares four cycles with the 3.5PN wave?

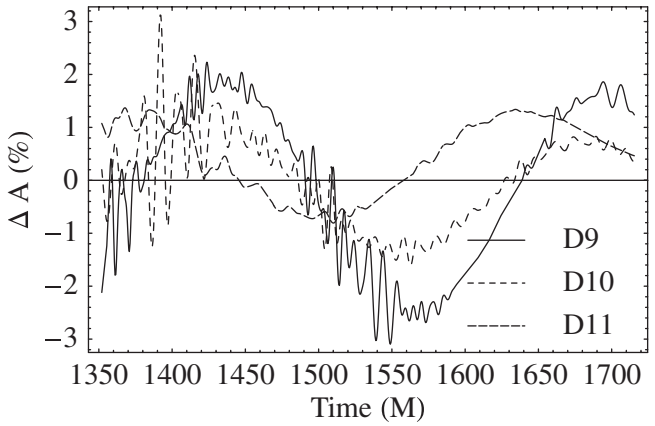

FIG. 14. The percentage difference in amplitude between the D12 simulation and the D9, D10, and D11 simulations. The D9, D10, and D11 amplitudes show small oscillations around the D12 value, but recall that the disagreement between the D12 and restricted 3.5PN amplitudes was 6%.

Figure 14 shows the relative disagreement in amplitude between the D12 simulation and the D9, D10, and D11 simulations. There are small oscillations around the D12 values, but these are smaller than the average amplitude disagreement between the NR and restricted 3.5PN wave amplitudes, and we expect that it will be possible to calculate a suitable scale factor for matching the NR and 3.5PN waves. We conclude then that simulations starting as close as $D = 9M$ and simulating about 4.5 orbits should be enough to match to restricted 3.5PN waveforms for many applications. To make this clearer: any GW data-analysis application that requires an amplitude accuracy of at most 5% up to the last four cycles, and an amplitude accuracy of better than 2% from that point through merger and ringdown, will require only short (4.5 orbit) numerical simulations to match to PN waveforms.

This result is attractive from a computational point of view. The D9 simulation ran in 750 CPU hours (two and a half days of wall clock time on 12 processors), while the highest resolution D12 simulation required 10 500 CPU hours (18 days on 24 processors). When producing many waveforms for use in gravitational-wave data analysis, we would much rather only have to perform the two-and-a-half-day simulations.

Of course, in the case of equal-mass binary inspiral, we have already presented waveforms that cover far more than four cycles before merger. The important question is whether similarly short simulations will be adequate beyond the equal-mass nonspinning case, and that will be the subject of future work.

C. Comparison with eccentric waveforms

The numerical simulations discussed in the previous sections modeled equal-mass inspiral with negligible eccentricity, starting from the initial parameters introduced in [27]. The eccentricity of the D12 simulation is estimated as

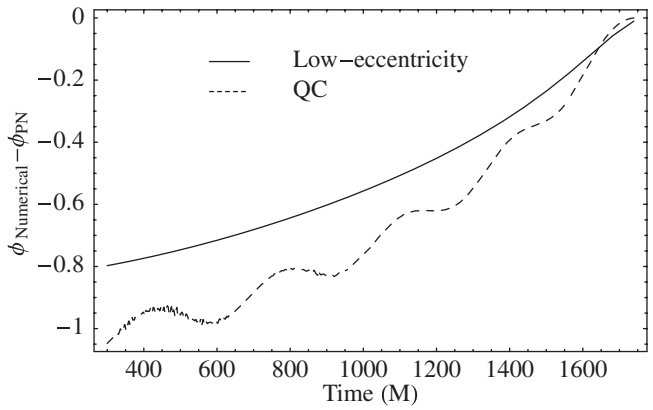

FIG. 15. The same quantities as in Fig. 9, this time comparing both the D12 and QC12 wave phase with that of the TaylorT1 3.5PN waves. The disagreement between the 3.5PN and QC phases displays clear oscillations, presumably due to the eccentricity in the QC12 simulation.

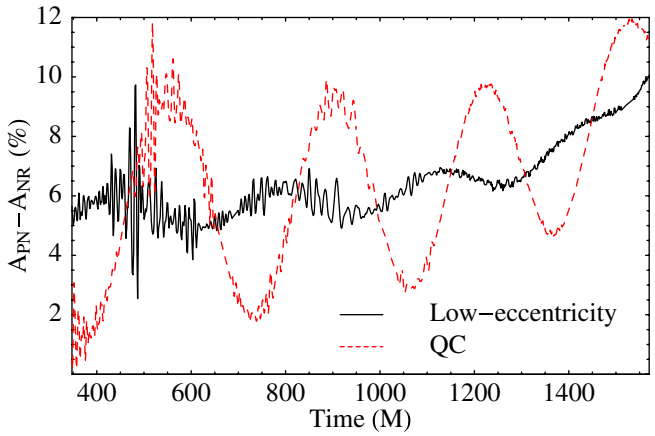

FIG. 16 (color online). Percentage disagreement between restricted PN and NR wave amplitudes, for both D12 and QC12 simulations. The disagreement between the QC12 and 3.5PN wave amplitudes is clearly dominated by eccentricity. The low-eccentricity D12 simulation is necessary to identify the error in the restricted PN wave amplitude.

$e < 0.0016$. In contrast, one could use standard "quasicircular orbit" parameters (i.e., parameters calculated with the assumption that $\dot{r} = 0$), which lead to inspiral with a small but noticeable eccentricity. We now consider a set of simulations with the same parameters as the D12 runs, but using initial parameters calculated using the 2PN-accurate expression used in [50] (and based on the results in [51]); we denote this simulation "QC12." We apply the same extrapolation procedure as described in Sec. IV to produce the final waveform that we analyze.

Figure 15 shows the same comparison with the TaylorT1 3.5PN wave phase as in the upper panel of Fig. 10, but now displaying results from both the D12 and QC12 simulations. The accumulated phase disagreement for the QC12 simulation is larger. The disagreement with the 3.5PN phase also shows oscillations that are presumably due to eccentricity. A similar effect can be seen in Fig. 16, which shows the percentage disagreement in wave amplitude. The amplitudes are now shown as functions of time; if we use $M\omega$ as before, the eccentricity effects are not visible. The low-eccentricity D12 waveform has been matched with the PN waveform at $M\omega = 0.0455$, and the QC12 waveform is matched with the D12 waveform so that their amplitude maxima occur at the same time. The amplitude disagreement between the D12 simulation and the restricted PN amplitude is slightly different than that shown in Fig. 13; this is due to parametrizing the amplitude with time instead of frequency—the PN/NR frequency disagreement means that there is not a 1-1 relationship between the two plots. However, the results are consistent within the 2% uncertainty in the numerical waveform amplitude.

The disagreement in amplitude between the restricted PN and QC12 results oscillates between 2% and 10% at early times. From the QC12 simulation alone, we may guess that the error in the restricted PN wave amplitude is the average of this curve, i.e., around 6%, but may also guess that the disagreement might go away if the eccentricity were removed. The D12 simulation, which displays far less eccentricity, confirms the first guess: there is strong numerical evidence that the restricted 3.5PN wave amplitude really does disagree with fully general-relativistic results by about 6%.

D. Comparison of the black-hole coordinate motion

To initialize our numerical simulations, we have set the initial momenta of the black holes to values we have obtained from a post-Newtonian inspiral calculation as described in [27]. The inspiral calculation starts at an initial separation of $D = 40M$ with momenta given by the 3PN-accurate quasicircular-orbit formula given in [13]. When

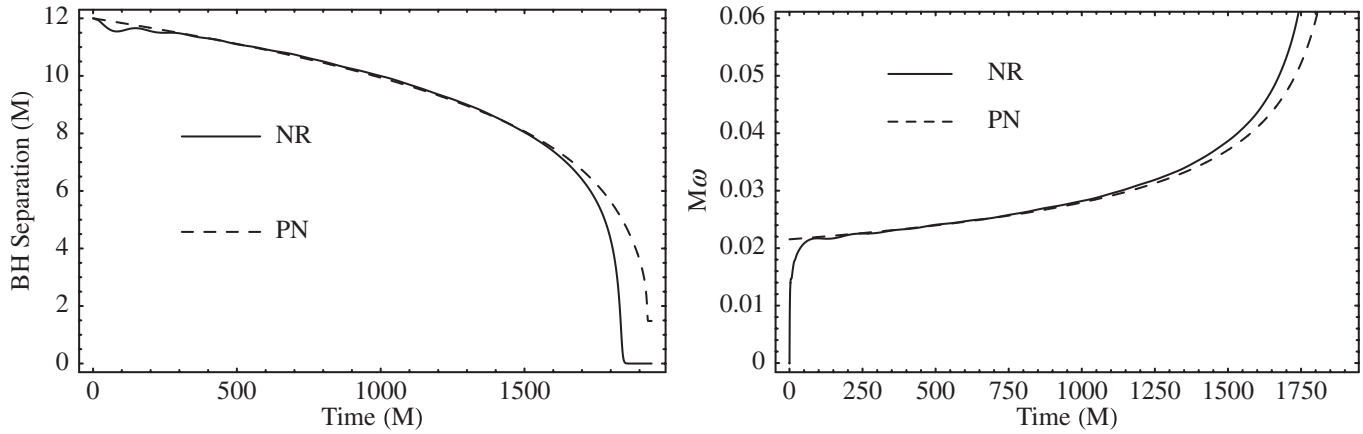

FIG. 17. Orbital coordinate motion of the D12 numerical-relativity evolution compared with a PN evolution with the same initial parameters. In both panels the PN evolution is drawn as a dashed line. Left panel: the separation of the black holes (the puncture position in the full NR case). Right panel: the coordinate angular velocity.

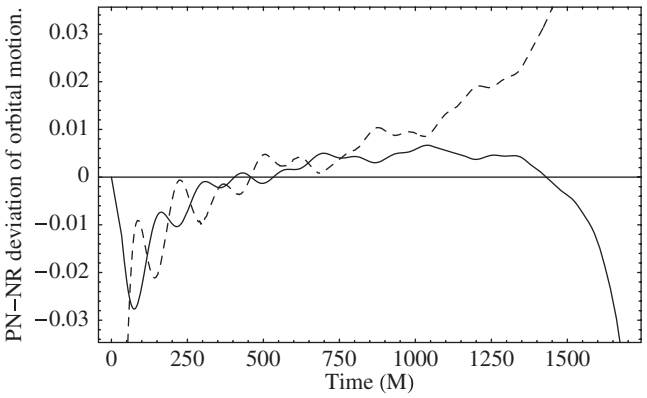

FIG. 18. Orbital coordinate motion of the D12 numerical-relativity evolution compared with a PN evolution with the same initial parameters. Dashed line: $(\omega_{\rm NR} - \omega_{\rm PN})/\omega_{\rm PN}$, full line: $(D_{\rm NR} - D_{\rm PN})/D_{\rm PN}$.

the inspiral reaches the separation $D = 12M$, the momenta are read off from the solution and given the values shown in Table II.

In this section we compare a full GR simulation that uses those parameters with continuing the PN inspiral from $D = 12M$.

The coordinate separation of the black-hole punctures was chosen as the coordinate separation of the post-Newtonian inspiral, which we have computed in ADM-transverse-traceless (ADMTT) coordinates. This is motivated by the fact that the PN solution in the ADMTT gauge for a two-body system agrees with our Bowen-York puncture initial data up to 2PN order (see, for example, the explicit solutions in Appendix A of [52]). It is therefore interesting to know when the use of the ADMTT gauge breaks down in our evolutions. An indirect check is straightforward: we compare the PN and full NR puncture separation, as seen in Figs. 17 and 18. Using the D12 simulation, we find that both the separation and orbital phase agree very well from $D = 11M$ up to $D = 8M$, or from $t = 300M$ (the time to complete the first orbit) to $t = 1500M$. Put another way, the PN and full NR coordinate separation agrees until about 3 orbits before merger.

VI. DISCUSSION

We have simulated nine orbits, merger, and ringdown of an equal-mass binary, and extracted waveforms of sufficient accuracy to make a detailed comparison with PN waveforms. The uncertainties in the numerical waveforms are dominated by the close extraction radii, and not finite-difference errors. The PN waveforms that we focused on were those generated by the TaylorT1 3.5PN procedure implemented in the LAL, which is a candidate for use in gravitational-wave searches in detector data; we also compared with the TaylorT3 approximant. We find that the phase of the TaylorT1 3.5PN waveform can be matched to agree with the numerical phase to within numerical uncertainties, and the upper bound of the accumulated phase disagreement is on the order of 1 rad. The restricted PN amplitude overestimates the numerical value $(6 \pm 2)\%$. We have found that the ratio of the restricted PN and NR wave amplitudes is roughly constant over the course of the evolution, and therefore an equally good matching between PN and NR waves should be possible with far less numerical cycles. In particular, we performed a simulation that completes only 4.5 orbits before merger, and expect that this could be used to produce hybrid waveforms by a procedure like that discussed in [24,25] or [21] just as well as a simulation that models many more cycles. We therefore conclude that, with the level of numerical accuracy that we can achieve, only about 4.5 orbits need be simulated for a PN/NR matching of the same accuracy. Whether these relatively modest requirements for numerical waveforms carry over to the cases of unequal-mass and spinning binaries will be the subject of future work.

For gravitational-wave detection we expect that such hybrid waveforms will be acceptable. However, for parameter estimation the issue of the discrepancy between the amplitude of PN and NR waveforms may have to be addressed. Modeling the amplitude at 2.5PN order gives agreement comparable to numerical error between PN and NR waves up to about 11 cycles before merger; at present we suggest that the best matching can be done with > 11 cycles (5.5 orbits) of numerical simulation. The cases where the current level of phase and amplitude accuracy are expected to be adequate for various data-analysis applications will also be explored in future work.

Comparing with evolutions of the PN equations of motion in the ADMTT gauge, we find that the orbital motion seen in the numerical evolutions agrees extremely well up to a coordinate separation of about $D = 8M$. This surprising agreement not only suggests that the PN dynamics accurately models the full physical dynamics up to about three orbits before merger, but that the numerical gauge remains close to the ADMTT gauge up to that time. In addition, the gauge dynamics and emission of junk radiation at the beginning of the simulation do not noticeably change either the dynamics or the gauge; after about one orbit the NR dynamics matches up again with the ADMTT PN dynamics.

ACKNOWLEDGMENTS

We thank Parameswaran Ajith, Duncan Brown, and Mark Scheel for alerting us to errors in old versions of the TaylorT1 routines in LAL, which were used to produce the results in an earlier draft of this paper. Since that draft was written, Duncan Brown has committed to the LAL cvs repository bug fixes to the relevant LAL routines. The subsequent changes in the TaylorT1 3.5PN waveform phase changed the accumulated phase disagreement in Fig. 10 from 0.15 radians to the current value of 0.8 radians. Prompted by these changes and by suggestions

from the anonymous journal referee, we extended our analysis. However, the main conclusions from the first draft are unchanged. We also thank Parameswaran Ajith and Alicia Sintes for helpful discussions regarding the use of the LAL library, Alessandra Buonanno and Achamveedu Gopakumar for clarifications regarding the TaylorT3 approximant, and Mark Scheel and Harald Pfeiffer for feedback regarding our matching techniques. This work was supported in part by DFG grant SFB/Transregio 7 ''Gravitational Wave Astronomy.'' We thank the DEISA Consortium (cofunded by the EU, FP6 Project No. 508830), for support within the DEISA Extreme Computing Initiative (www.deisa.org). Computations were performed at LRZ Munich and the Doppler and Kepler clusters at the Institute of Theoretical Physics of the University of Jena. M. H. and S. H. gratefully acknowledge hospitality of the University of the Balearic Islands.

Note.—While this article was undergoing peer review, the Caltech/Cornell group completed a detailed PN/NR comparison that covers 30 gravitational-wave cycles (15 orbits) before merger with high numerical accuracy in their numerical waveforms [53]. Where comparable, their results confirm those in this paper; a comparison between our results and theirs is provided in their paper.

[1] S. Waldman (LIGO Scientific Collaboration), Classical Quantum Gravity **23**, S653 (2006).
[2] S. Hild (LIGO Scientific Collaboration), Classical Quantum Gravity **23**, S643 (2006).
[3] F. Acernese *et al.*, Classical Quantum Gravity **23**, S635 (2006).
[4] A. Buonanno, Y. Chen, and M. Vallisneri, Phys. Rev. D **67**, 024016 (2003); **74**, 029903(E) (2006).
[5] Lsc algorithm library (LAL), URL: http://www.lsc-group.phys.uwm.edu/lal.
[6] F. Pretorius, Phys. Rev. Lett. **95**, 121101 (2005).
[7] M. Campanelli, C. O. Lousto, P. Marronetti, and Y. Zlochower, Phys. Rev. Lett. **96**, 111101 (2006).
[8] J. G. Baker, J. Centrella, D.-I. Choi, M. Koppitz, and J. van Meter, Phys. Rev. Lett. **96**, 111102 (2006).
[9] F. Pretorius, Classical Quantum Gravity **23**, S529 (2006).
[10] M. Campanelli, C. O. Lousto, and Y. Zlochower, Phys. Rev. D **73**, 061501(R) (2006).
[11] J. G. Baker, J. Centrella, D.-I. Choi, M. Koppitz, and J. van Meter, Phys. Rev. D **73**, 104002 (2006).
[12] U. Sperhake, Phys. Rev. D **76**, 104015 (2007).
[13] B. Brügmann, J. A. González, M. Hannam, S. Husa, U. Sperhake, and W. Tichy, arXiv:gr-qc/0610128.
[14] J. G. Baker, S. T. McWilliams, J. R. van Meter, J. Centrella, D.-I. Choi, B. J. Kelly, and M. Koppitz, Phys. Rev. D **75**, 124024 (2007).
[15] J. G. Baker, J. R. van Meter, S. T. McWilliams, J. Centrella, and B. J. Kelly, Phys. Rev. Lett. **99**, 181101 (2007).
[16] H. P. Pfeiffer, D. Brown, L. E. Kidder, L. Lindblom, G. Lovelance, and M. A. Scheel, Classical Quantum Gravity **24**, S59 (2007).
[17] M. A. Scheel, H. P. Pfeiffer, L. Lindblom, L. E. Kidder, O. Rinne, and S. A. Teukolsky, Phys. Rev. D **74**, 104006 (2006).
[18] S. Husa, J. A. González, M. Hannam, B. Brügmann, and U. Sperhake, arXiv:0706.0740.
[19] A. Buonanno, G. B. Cook, and F. Pretorius, Phys. Rev. D **75**, 124018 (2007).
[20] E. Berti *et al.*, Phys. Rev. D **76**, 064034 (2007).
[21] Y. Pan *et al.*, arXiv:0704.1964 [Phys. Rev. D (to be published)].
[22] A. Buonanno, Y. Pan, J. G. Baker, J. Centrella, B. J. Kelly, S. T. McWilliams, and J. R. van Meter, Phys. Rev. D **76**, 104049 (2007).
[23] B. Vaishnav, I. Hinder, F. Herrmann, and D. Shoemaker, Phys. Rev. D **76**, 084020 (2007).
[24] P. Ajith, S. Babak, Y. Chen, M. Hewitson, B. Krishnan, J. T. Whelan, B. Brügmann, P. Diener, J. González, M. Hannam *et al.*, Classical Quantum Gravity **24**, S689 (2007).
[25] P. Ajith *et al.*, arXiv:0710.2335.
[26] A. Buonanno, Y. Chen, and T. Damour, Phys. Rev. D **74**, 104005 (2006).
[27] S. Husa, M. Hannam, J. A. González, U. Sperhake, and B. Brügmann, arXiv:0706.0904.
[28] B. Brügmann, W. Tichy, and N. Jansen, Phys. Rev. Lett. **92**, 211101 (2004).
[29] S. Brandt and B. Brügmann, Phys. Rev. Lett. **78**, 3606 (1997).
[30] J. M. Bowen and J. W. York, Phys. Rev. D **21**, 2047 (1980).
[31] M. Ansorg, B. Brügmann, and W. Tichy, Phys. Rev. D **70**, 064011 (2004).
[32] M. Campanelli, C. O. Lousto, P. Marronetti, and Y. Zlochower, Phys. Rev. Lett. **96**, 111101 (2006).
[33] J. G. Baker, J. Centrella, D.-I. Choi, M. Koppitz, and J. van Meter, Phys. Rev. Lett. **96**, 111102 (2006).
[34] M. Shibata and T. Nakamura, Phys. Rev. D **52**, 5428 (1995).
[35] T. W. Baumgarte and S. L. Shapiro, Phys. Rev. D **59**, 024007 (1998).
[36] J. W. York, in *Sources of Gravitational Radiation*, edited by L. L. Smarr (Cambridge University Press, Cambridge, England, 1979), p. 83, ISBN 0-521-22778-X.
[37] W. Tichy and B. Brügmann, Phys. Rev. D **69**, 024006 (2004).
[38] G. B. Cook and J. W. York, Jr., Phys. Rev. D **41**, 1077 (1990).
[39] G. B. Cook, Ph.D. thesis, University of North Carolina at Chapel Hill, Chapel Hill, North Carolina, 1990.
[40] M. Campanelli, C. O. Lousto, and Y. Zlochower, Phys. Rev. D **74**, 084023 (2006).
[41] T. Damour, B. R. Iyer, and B. S. Sathyaprakash, Phys. Rev.

D **63**, 044023 (2001).Phys. Rev. D**72**, 029902(E) (2005).
[42] T. Damour, B. R. Iyer, and B. S. Sathyaprakash, Phys. Rev. D **66**, 027502 (2002).**72**, 029901(E) (2005).
[43] K. Arun, L. Blanchet, B. R. Iyer, and M. S. S. Qusailah, Classical Quantum Gravity **21**, 3771 (2004). **22**, 3115(E) (2005).
[44] L. Blanchet, T. Damour, G. Esposito-Farese, and B. R. Iyer, Phys. Rev. Lett. **93**, 091101 (2004).
[45] L. Blanchet, G. Faye, B. R. Iyer, and B. Joguet, Phys. Rev. D **65**, 061501 (2002).**71**, 129902(E) (2005).
[46] P. A. Sundararajan, G. Khanna, and S. A. Hughes, Phys. Rev. D **76**, 104005 (2007).
[47] B. Krishnan, C. O. Lousto, and Y. Zlochower, Phys. Rev. D **76**, 081501 (2007).
[48] C. O. Lousto and Y. Zlochower, arXiv:0708.4048 [Phys. Rev. D (to be published)].
[49] D. R. Fiske, J. G. Baker, J. R. van Meter, D. Choi, and J. M. Centrella, Phys. Rev. D **71**, 104036 (2005).
[50] B. Brügmann, J. A. González, M. Hannam, S. Husa, and U. Sperhake (unpublished).
[51] L. E. Kidder, Phys. Rev. D **52**, 821 (1995).
[52] P. Jaranowski and G. Schäfer, Phys. Rev. D **57**, 7274 (1998).
[53] M. Boyle *et al.*, arXiv:0710.0158 [Phys. Rev. D (to be published)].